Inhibition of Amyloid Aggregation by Formation of Helical Assemblies

ARTICLE *in* CHEMISTRY - A EUROPEAN JOURNAL · SEPTEMBER 2011

Impact Factor: 5.73 · DOI: 10.1002/chem.201100670 · Source: PubMed

5 AUTHORS, INCLUDING:

Enrico Brandenburg
Freie Universität Berlin
10 PUBLICATIONS **45** CITATIONS
SEE PROFILE

Ulla I M Gerling
Freie Universität Berlin
11 PUBLICATIONS **130** CITATIONS
SEE PROFILE

Beate Koksch
Freie Universität Berlin
113 PUBLICATIONS **1,762** CITATIONS
SEE PROFILE

DOI: 10.1002/chem.201100670

Inhibition of Amyloid Aggregation by Formation of Helical Assemblies

Enrico Brandenburg,[a] Hans von Berlepsch,[b] Ulla I. M. Gerling,[a] Christoph Böttcher,[b] and Beate Koksch*[a]

Abstract: The formation of amyloid aggregates is responsible for a wide range of diseases, including Alzheimer's and Parkinson's disease. Although the amyloid-forming proteins have different structures and sequences, all undergo a conformational change to form amyloid aggregates that have a characteristic cross-β-structure. The mechanistic details of this process are poorly understood, but different strategies for the development of inhibitors of amyloid formation have been proposed. In most cases, chemically diverse compounds bind to an elongated form of the protein in a β-strand conformation and thereby exert their therapeutic effect. However, this approach could favor the formation of prefibrillar oligomeric species, which are thought to be toxic. Herein, we report an alternative approach in which a helical coiled-coil-based inhibitor peptide has been designed to engage a coiled-coil-based amyloid-forming model peptide in a stable coiled-coil arrangement, thereby preventing rearrangement into a β-sheet conformation and the subsequent formation of amyloid-like fibrils. Moreover, we show that the helix-forming peptide is able to disassemble mature amyloid-like fibrils.

Keywords: aggregation · amyloid inhibition · coiled coils · protein folding · self-assembly

Introduction

Many neurodegenerative diseases, such as Alzheimer's disease, type II diabetes, Parkinson's disease, and Creutzfeldt–Jacob disease, are linked to the failure of a peptide or protein to fold correctly or to remain in its functional conformational state.[1–3] Instead, there is a conformational change from the native state to highly organized, β-sheet-rich amyloid fibrils. The mechanism involves a multistep process, in which unstable prefibrillar oligomers assemble into protofibrils and further into amyloid fibrils. Early work regarding the toxicity of these species focused on the amyloid fibrils, but recent studies have suggested that the prefibrillar oligomers are the main cytotoxic species.[4–9] The exact causal relationship between amyloid formation and each disease is still not understood.

Besides the elucidation of the molecular mechanisms involved in amyloidogenesis, recent research has been concentrated on the search for suitable inhibitors of this process. The screening of libraries of small molecules[10,11] and the rational design of peptides[12–14] have led in most cases to inhibitors that bind to aggregated species and prevent further polymerization by blocking the addition of peptide monomers.[15,16] Numerous studies on the development of peptide-based amyloid aggregation inhibitors have taken the core sequence of the target peptide as a lead as it is already known to bind to itself. The peptide-based inhibitors were designed to bind to the peptide backbone in β-sheet conformation. They block further elongation by steric effects, electrostatic repulsion, or inhibition of the formation of hydrogen bonds.[17–19] However, blocking fibril formation by this strategy could increase the number of prefibrillar oligomeric forms, which are thought to be the toxic species in the amyloid-formation process.[6] Therefore, alternative approaches are necessary. The conversion from the soluble monomeric form into various β-sheet-rich aggregated morphologies appears to be the key event.[20] Therefore, prevention of this conversion may offer a promising approach to therapy. Recently, studies on small molecule inhibitors have shown that they can prevent the aggregation of transthyretin by stabilizing its native state.[21] In other studies, attempts have been made to redirect the mechanism of folding to presumably non-toxic assemblies by using molecular chaperones and small molecules.[22,23] Several naturally occurring amyloidogenic peptides that form β-sheet-rich fibrils harbor an α-helix in the primary structure, such as prion protein (helix 2, positions 179–191) and the Aβ-peptide (16–23), which are described as α/β-discordant helices.[24] Moreover, according to systematic studies on several amyloidogenic proteins and peptides, including the Aβ peptide,[25–28] IAPP,[29,30] tau protein,[31] α-synuclein (αS),[32] glutamine/asparagines (Q/N)-rich prions as well as polyQ-expanded huntingtin,[33] and several de novo designed fragments derived from globular proteins,[34] these molecules appear to form helical inter-

[a] E. Brandenburg, U. I. M. Gerling, Prof. Dr. B. Koksch
Institut für Chemie und Biochemie, Freie Universität Berlin
Takustrasse 3, 14195 Berlin (Germany)
Fax: (+49) 30-838-44644
E-mail: koksch@chemie.fu-berlin.de

[b] Dr. H. von Berlepsch, Dr. C. Böttcher
Forschungszentrum für Elektronenmikroskopie, Freie Universität Berlin, Fabeckstrasse 36a, 14195 Berlin (Germany)

Supporting information for this article is available on the WWW under http://dx.doi.org/10.1002/chem.201100670.

mediates during amyloid formation under certain conditions. It was suggested that these helical segments might be stabilized in their helical conformation in order to prevent the formation of amyloid structures.[35–38] For example, the region 13–26 of the Aβ peptide can serve as a target for obtaining a successful design of specific helix-stabilizing inhibitors, as Nerelius et al. showed recently.[39]

In the present study, we investigated the potential of this approach by using model peptides that were more advantageous than naturally occurring peptides. Simplified model peptides were developed because the structural transitions that occur in natural systems are extraordinarily complex processes and are therefore still only partially understood on a molecular level.[40] Model systems can overcome these and other drawbacks of natural systems, such as low solubility and poor synthetic accessibility. Moreover, they can help to elucidate the molecular interactions that occur during structural transition and the formation of amyloid fibrils, and more importantly they can provide insights into different strategies for inhibiting amyloid formation.[41–43] We recently designed and synthesized a series of 26-residue model peptides that were based on the characteristic heptad repeat of the α-helical coiled-coil motif. By incorporating valine residues at three different solvent-exposed positions, the system was made more prone to amyloid formation.[44,45] The conformational transition and the obtained amyloid-like structures were thoroughly characterized. To summarize this previous work, we were able to design model peptides that adopted different conformations and aggregate morphologies depending on the concentration, pH, ionic strength, and the presence of metal ions or other triggers.[46–50] Our earlier success in the rational design of amyloidogenic model peptides encouraged us to investigate strategies to inhibit aggregation. As discussed in detail above, one promising approach is the preclusion of amyloid formation by stabilization of the helical conformation of a target peptide through the formation of stable assemblies. By means of the de novo design approach, we showed that a coiled-coil-based amyloidogenic target peptide that shows α/β-discordance could become engaged in a stable helical arrangement in the presence of an idealized helical coiled-coil model peptide as an alternative to adopting a β-sheet conformation and ultimately forming amyloid structures. Moreover, this ideal coiled-coil model peptide is able to disassemble amyloid-like fibrils once they have already formed.

Results

Peptide design: From the series of model peptides developed in recent years[44,46,48,50,51] we chose the peptides VW01 and VW18 (Figure 1) as representatives of an idealized coiled-coil and amyloid-forming peptide, respectively. The design of both model peptides is based on the well known and highly versatile α-helical coiled-coil folding motif.[52] Coiled-coil peptides consist of two to five α-helices, which are wrapped around each other to form a left-handed super-

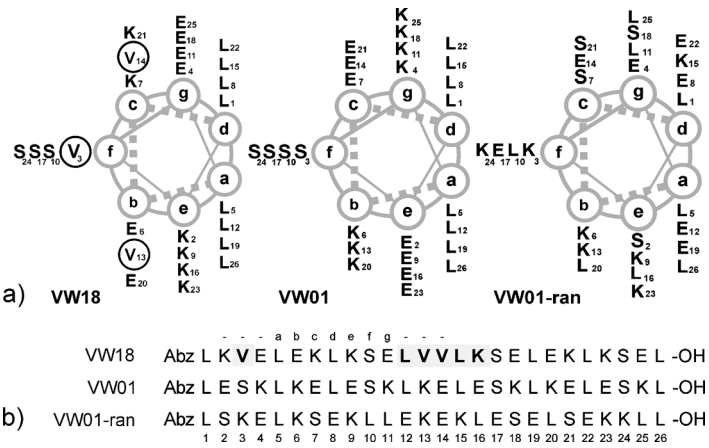

Figure 1. a) Helical wheel diagram and b) sequences of peptides VW18, VW01, and VW01-ran. The circle joins the b, c, and f positions occupied by valines that make peptide VW18 prone to β-sheet formation. The positively charged residues are marked in blue, the negatively charged residues in red.

helix.[53,54] The primary sequence of the α-helix is characterized by repeats of seven residues, commonly designated by the letters a to g. Positions a and d are exclusively occupied by hydrophobic leucine residues, forming the first recognition motif by hydrophobic core packing. Charged glutamate and lysine residues are present in positions g and e and are engaged in favorable electrostatic interactions in the case of a parallel helix alignment. Thus, electrostatic interactions form the second recognition motif, which contributes to stability and determines the specificity of folding. The positions b, c, and f of the heptad are solvent-exposed. VW01 and VW18 have intact first and second recognition motifs, which is necessary for stable coiled-coil formation. The major difference between the two peptides is the replacement of three polar residues in positions b, c, and f by β-sheet-preferring valine residues, resulting in VW18.

Thus, VW18 contains two competing secondary structure motifs. The principle of this design was also supported by the computer algorithms TANGO and AGADIR.[55,56] TANGO is able to identify aggregation-prone regions in the primary sequence and indicate competing structural propensities, such as for helix or β-sheet formation.[56] The output for the primary sequence of VW18 showed that the LVVLK sequence was the aggregation-prone sequence, which is comparable to the amyloid stretch KLVFF of the Aβ peptide (Figure S1 in the Supporting Information). On the basis of the amyloid stretch hypothesis, these segments provide the main driving force in triggering amyloid formation.[58] However, the replacement of polar residues by β-sheet-preferring residues, which leads to decreased helicity compared to VW01, as indicated by a higher random coil content in the case of VW18, also influenced their tendency to form amyloid-like fibrils.[28] The output of the AGADIR algorithm also showed reduced helical content compared to VW01.

In summary, this reflects the idea of designing a peptide with competing structural motifs and the creation of similar α/β-discordance as is described for the naturally occurring amyloidogenic peptides mentioned in the introduction. Therefore, VW18 is a suitable model peptide to investigate the potential of the approach of targeting the helical segment to prevent amyloid formation.

With regard to the coiled-coil design and the concept of inhibition, we can say that two of the three solvent-exposed valine residues within the coiled-coil sequence provided the possibility for β-sheet formation, while the two intact recognition motifs formed by the amino acids in positions a, d, e, and g enabled the α-helical arrangement. These positions can be targeted by a complementary sequence that will form a complex with VW18 and result in a stable helical fold. To demonstrate that the impact of inhibitor VW01 could only be attributed to the coiled-coil formation, a control peptide was synthesized. The control peptide VW01-ran had the same amino acid composition as VW01, but the primary sequence was randomized and did not contain the characteristic heptad repeat. This peptide had no intact hydrophobic or electrostatic recognition motifs and was not able to form a stable coiled coil.

Characterization of the pure peptides: First, the folding behaviors of both the target and inhibitor peptides were characterized to determine the inhibition effect. The presence of valine residues at positions b, c, and f made the target peptide VW18 prone to form β-sheet structures. Circular dichroism (CD) measurement (Figure 2a) revealed a conformational change from an α-helical, indicated by two minima at 208 and 222 nm, to a β-sheet conformation, with a typical minimum at 218 nm, within only about 15 h at pH 7.4.

Thioflavin T (ThT) fluorescence experiments (Figure 2b) showed a time-dependent enhancement of the fluorescence signal at around 485 nm that could best be described by a sigmoidal curve with a characteristic lag time of ~5 h. This behavior is typical of many amyloid-forming peptides and suggests a nucleation-dependent process of fibrillar growth.[59,60] The images obtained from electron microscopic studies of the morphology were consistent with this interpretation. Figure 3(a, b) present micrographs of negatively stained and cryo-TEM preparations of a matured solution, respectively, which revealed helically twisted fibrils that were several hundreds of nanometers long and approximately 10 nm wide. Additional X-ray fibre diffraction studies (Figure S2 in the Supporting Information) confirmed the expected cross-β-structure. The diffraction patterns consisted of two major reflections, a sharp meridional reflection at 4.7 Å corresponding to the hydrogen-bonding distance between β-strands in a β-sheet, and a more diffuse equatorial reflection at around 10 Å due to the lateral spacing between the β-sheets stacked within the fibril. In contrast to VW18, the inhibitor peptide VW01 adopted a helical conformation, indicated by two clear CD minima at 208 and 222 nm (Figure 2c), and did not undergo changes in its conformation over the pH range 4–9, a concentration range of 100–500 μM, or incubation times of up to 5 days (data not shown). The absence of a ThT fluorescence enhancement (Figure 2b) in this case was consistent with the CD findings. Cryo-TEM studies on a 100 μM peptide solution revealed small particles with a typical size of 2.5–3.0 nm (Figure 3c). At high peptide concentrations (>300 μM), a few thread-like fibrillar aggregates of diameter 2.5±0.3 nm and length 50–100 nm were additionally detected.

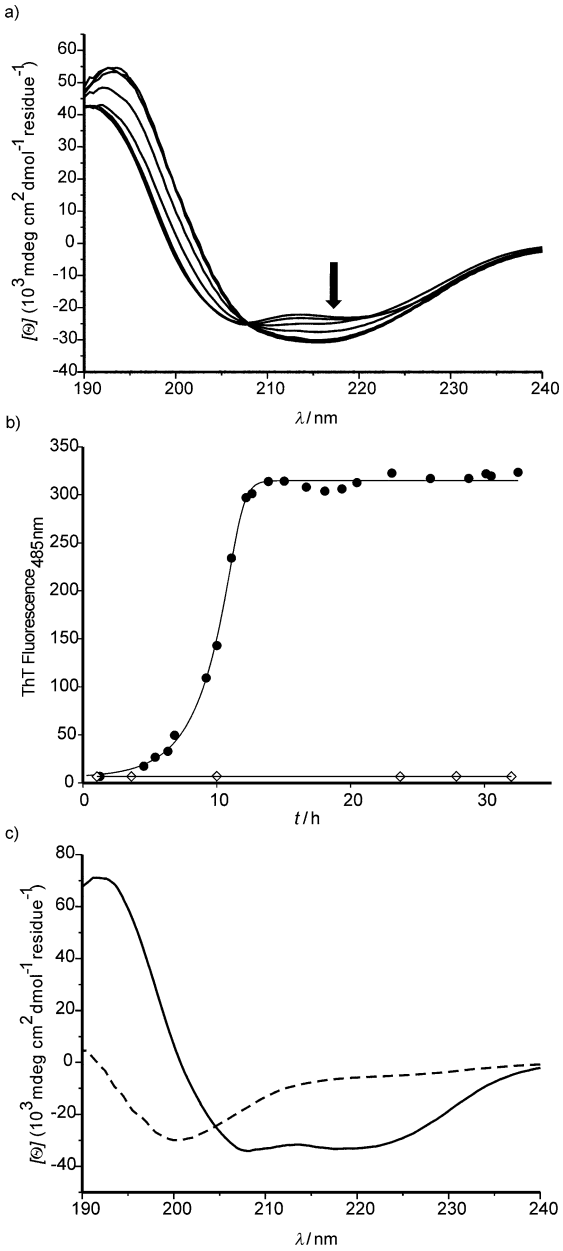

Figure 2. Time-dependent conformational change. All samples contained 100 μM peptide and were prepared in 10 mM phosphate buffer at pH 7.4. a) Overlaid CD spectra of peptide VW18 for different incubation times up to 50 h. b) ThT-staining assays (10 μM ThT) of peptide VW18 (●) and VW01 (◇) as a function of incubation time. c) Representative CD spectra of peptides VW01 and VW01-ran that are stable for extended periods of time.

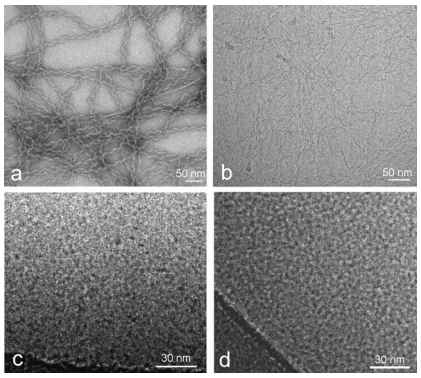

Figure 3. Electron micrographs of pure peptides. The VW18 and VW01 samples contained 100 μM peptide and were prepared in 10 mM phosphate buffer at pH 7.4. a) TEM micrograph of PTA-stained helically twisted fibrils of peptide VW18 after two days of incubation. b) Respective cryo-TEM micrograph of a VW18 solution. c) Cryo-TEM micrograph of a VW01 solution after 5 days of incubation, revealing oligomers but no higher aggregates. d) Cryo-TEM micrograph of a 500 μM VW01-ran solution in 10 mM phosphate buffer at pH 7.4 showing oligomers.

The oligomerization state is an important structural parameter in the formation of coiled-coil assemblies that is not strictly predictable by the design.[61,62] Therefore, the oligomerization state of the inhibitor VW01 was experimentally determined by analytical ultracentrifugation (AUZ). We ran both sedimentation velocity (SV) and sedimentation equilibrium (SE) experiments. The SV experiment gave a molecular mass of $M_w = 9923\ g\,mol^{-1}$ for a 20 μM peptide solution and $M_w = 9977\ g\,mol^{-1}$ for a 300 μM peptide solution. Considering the theoretical peptide mass of $M_{w(theo)}$ (VW01) = $3190\ g\,mol^{-1}$, these data suggested that VW01 assembled into trimers at both concentrations. An additional small population of presumably hexamers became visible at 300 μM (Figure S3 in the Supporting Information). This indicated a growth of the VW01 assemblies at higher peptide concentrations and confirmed the TEM results.

The data in SE experiments were collected at two rotor speeds (25000 and 30000 rpm) at peptide concentrations ranging from 20 to 500 μM. WINNONLIN[63] was used to analyze the data. The data were fitted globally to a model of non-interacting ideal species over the entire investigated concentration range, giving $M_w = 9706\ g\,mol^{-1}$ (25000 rpm) and $M_w = 9757\ g\,mol^{-1}$ (30000 rpm), which again suggested the formation of trimers (Figures S4 and S5, Table S2 in the Supporting Information).

The CD spectrum of the control peptide VW01-ran showed a minimum at 200 nm, which is characteristic of an unfolded structure (Figure 2c). Cryo-TEM studies on a 500 μM peptide sample revealed small particles with a typical size in the 2.5–3.0 nm range (Figure 3d). Higher aggregates could not be detected even at this concentration. That VW01-ran oligomerizes at all was ruled out by analytical ultracentrifugation. The SV experiments gave a molecular mass of $M_w = 2940\ g\,mol^{-1}$ for a 150 μM peptide solution. Comparison with the theoretical peptide molecular mass ($3190\ g\,mol^{-1}$) pointed to monomeric particles (Figure S6 in the Supporting Information). A concentration-enhanced assembly into higher aggregates could be excluded by SV measurements at higher peptide concentrations. Additional SE data were collected at two rotor speeds (30000 rpm and 50000 rpm) for peptide concentrations ranging from 20 to 150 μM. The MSTAR[64] program was used to analyze the data. Their global fit to a model of non-interacting ideal species over the entire investigated concentration range gave molecular masses of $M_w = 3383$ and $3093\ g\,mol^{-1}$ for the rotor speeds of 30000 and 50000 rpm, respectively, and confirmed the results of the SV experiments (Figure S7 in the Supporting Information). In summary, all of the obtained structural data indicate that the designed control peptide VW01-ran indeed behaves in the expected way, that is, it adopts a random coil conformation and does not form oligomers.

Inhibition of amyloid formation: The effect of VW01 on VW18 fibril formation was monitored by CD spectroscopy, ThT fluorescence, and by morphological investigations using electron microscopy. To examine the inhibition efficiency, VW01 was added at three different [VW18]/[VW01] molar ratios, $r[18/01]$, of 3, 2, and 1 to a fixed amount of 100 μM VW18.

The CD spectra (Figure S8 in the Supporting Information) revealed two clear minima at 208 and 222 nm over the total incubation period of five days at both $r[18/01] = 2$ and 1, which is indicative of stable helical conformations; β-sheet formation seems to be prevented under these conditions. However, with a large excess of VW18, that is, for $r[18/01] = 3$, no inhibition effect was observed. The two minima disappeared within two days and became replaced by a single minimum at around 218 nm. Although the CD effect was much weaker than in the case of pure VW18, this behavior clearly indicated the formation of β-sheets. To further prove the inhibition effect of VW01, we performed ThT fluorescence measurements.

Figure 4a shows the time courses of fibril formation in the presence of different amounts of VW01, monitored by means of ThT fluorescence. It is evident that adding the stable helical coiled-coil peptide VW01 to the amyloid-forming model peptide VW18 before aggregation had a concentration-dependent inhibitory effect. Thus, at an equimolar ratio ($r[18/01] = 1$), the ThT fluorescence intensity was almost zero, that is, inhibition was nearly complete, while the intensity at $r[18/01] = 2$ was reduced by 95%, and at $r[18/01] = 3$ by approximately one-third. These measurements confirmed the results of the CD investigations. TEM micrographs of respective VW18 solutions incubated either in the absence or in the presence of VW01 ($r[18/01] = 1$) are shown in Figure 4c). The micrographs were taken after five days of incubation. The typical amyloid fibrils formed by pure VW18 (Figure 4(c, upper panel)) were no longer found when VW01 was present, but were replaced by nanometer-sized, spot-like particles (Figure 4(c, lower panel)). The images support the spectroscopic results and verify the inhibition of fibrillization.

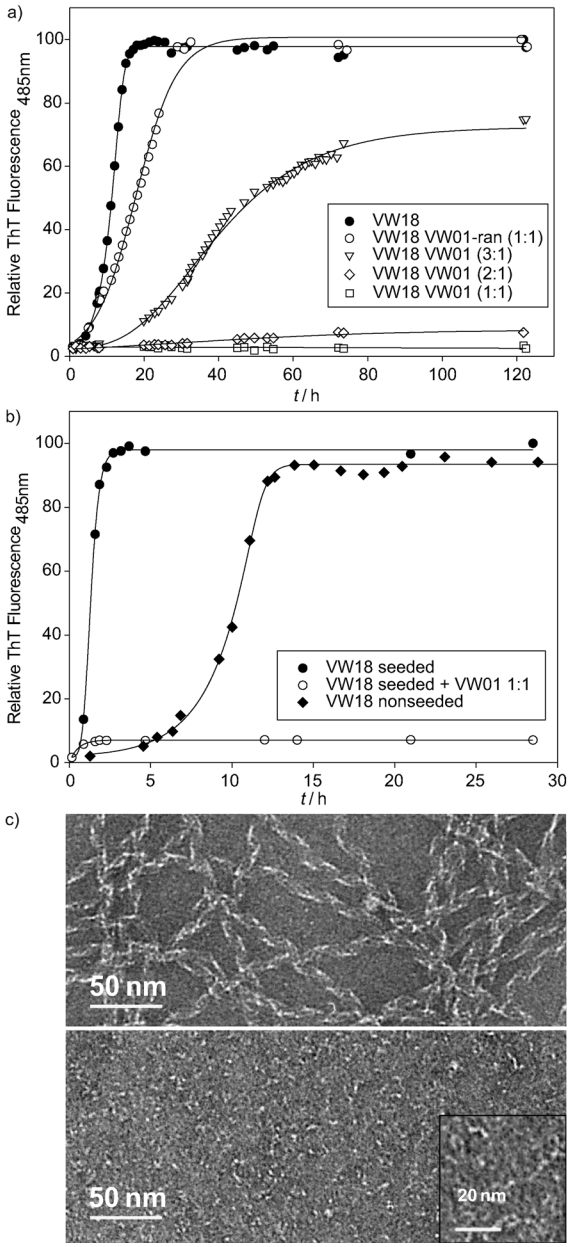

Figure 4. a) ThT-staining assays (10 μM ThT) of the inhibition of fibril formation of VW18 (100 μM in 10 mM phosphate buffer at pH 7.4) after addition of VW01 or VW01-ran at the molar ratios indicated. b) ThT-staining assay of the seeded aggregation of VW18 alone (●) and in the presence of one molar equivalent of VW01 (○). For comparison, the aggregation time course of non-seeded VW18 (◆) monitored by the ThT fluorescence is also shown. Negative-stain TEM micrographs of incubated samples prepared in 10 mM phosphate buffer at pH 7.4 containing c) 100 μM VW18 alone (above) and in the presence of one molar equivalent of VW01 (below). When VW01 was present during incubation, the helically twisted fibrils that are typical of the pure peptide VW18 were replaced by spot- or worm-like small oligomeric particles at higher magnification (inset).

We also probed the effect of the randomized peptide VW01-ran on the VW18 fibrillization process. The ThT fluorescence assay for an equimolar VW18/VW01-ran mixture showed a similar fluorescence growth rate and no reduction in the final fluorescence level as compared with the pure VW18 sample (Figure 4a). This finding shows that the helical secondary structure of the peptide VW01 is a necessary condition for its inhibitory effect. We conclude that complementary interactions provided by the heptad repeat may be involved and lead to the formation of soluble coiled-coil off-pathway oligomers.

It is well known that the amyloid-forming reaction can be accelerated by the addition of small amounts of preformed fibrils to a soluble sample of the amyloid-forming peptide. The added seed acts as a template that eliminates the lag phase during the fibrillogenesis. To ascertain whether such effects reduced the potential of the peptide VW01 to inhibit the VW18 fibrillization, we conducted respective seeding experiments in the absence or in the presence of VW01 (Figure 4b). A ThT assay revealed that the lag phase during the fibrillization process of pure VW18 was indeed eliminated by the addition of 5% (v/v) preformed fibrils at the beginning of incubation. A second effect of seeding was a slightly enhanced growth rate. Impressively, in the case of equimolar VW18/VW01 mixtures with seeding, no fluorescence-enhancing effect was observed and the inhibition was almost complete.

Disassembly of mature fibrils: Despite the extreme stability of amyloid fibrils towards proteases, acids, or chemical denaturants, an increasing number of studies have indicated that the process of amyloid formation is reversible.[65,66] Such findings stimulated the search for strategies aimed at the disruption of amyloid fibrils[67–69] and it became obvious that it would be advantageous to investigate the capacity of VW01 to dissolve mature VW18 amyloid structures.

A VW18 stock solution containing ThT was prepared and incubated. The ThT fluorescence intensity reached a maximum within 24 h of incubation, indicating that fibril formation was complete at this point (Figure 5a). Subsequently, the solution was split into three parts. One part was left unmodified to serve as a control. To the other two parts aliquots of either VW01 or VW01-ran solutions were added up to molar ratios of $r[18/01]=0.2$ and $[VW18]/[VW01\text{-ran}]=0.2$, respectively. The fluorescence intensity was followed for a further seven days of incubation. The obtained time courses are displayed in Figure 5a.

Comparison of the kinetic curves shows a rapid decrease in fluorescence intensity by about 60% immediately after the addition of the inhibitor peptide VW01 and by about 20% when VW01-ran was added. Negative-stain TEM micrographs of the solutions were taken after eight days of incubation. The aggregates of the control solution (Figure 5b) possessed the typically twisted, filamentous morphology of pure VW18 solutions. The image of the VW18/VW01 mixture (Figure 5d) revealed substantially disturbed fibrils and populations of small non-fibrillar aggregates. The small aggregates could represent oligomeric VW18/VW01 assemblies, but a fraction certainly consisted of oligomers formed by free peptide VW01 in view of its large excess over peptide VW18. On the other hand, the decoration of the fibril-

lar objects with smaller particles seems to be a clear indication of a strong interaction between the two peptides. Although it is difficult to quantify the extent of aggregation by electron microscopy, the detected morphological changes qualitatively supported the ThT fluorescence measurements, which indicated a partial dissolution of VW18 amyloid fibrils after addition of the peptide VW01. Additional support came from the sample that contained the sequence-randomized peptide VW01-ran. For this sample, TEM revealed small particles spread over seemingly intact amyloid fibrils (Figure 5d).

The morphological investigation confirmed the findings from the ThT fluorescence measurement (Figure 5a), which ruled out an effective interaction between VW01-ran and VW18 in its soluble or aggregated state. The gradual decrease in the ThT fluorescence intensity in the latter case could be due to a partial displacement of bound ThT molecules.

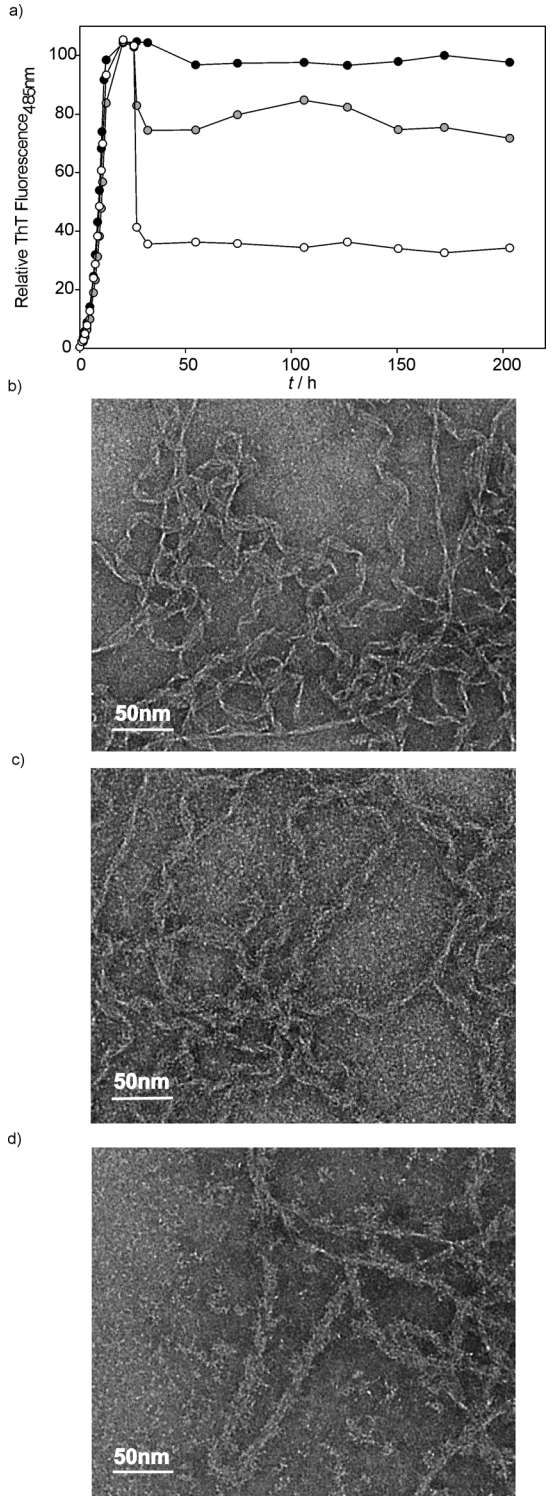

Figure 5. Disassembly of VW18 fibrils. ThT-staining assay a) of VW18 alone (● black), with the inhibitor VW01 (○), and with VW01-ran (● grey). Negative-stain TEM micrographs of VW18 incubated for 8 d alone (b), with VW01-ran present at r18/01 = 0.2 (c), and with VW01 present at [VW18]/[VW01] = 0.2 (d).

Oligomerization state: Because the oligomerization state of the isolated peptides and peptide–inhibitor complexes is crucial for the interpretation of the experiments, extended AUC and size-exclusion chromatography (SEC) experiments were carried out to obtain quantitative data. Although pure preparations of VW01 and VW01-ran are amenable to characterization by AUC, mixtures containing the amyloidogenic peptide could only be investigated by means of SEC because centrifugation led to unwanted aggregation. The addition of Abz-Gly to all SEC samples allowed for a precise calibration of retention times. As further references, the retention times of VW01 and VW01-ran were used, because their oligomerization states are known from AUC measurements.

The size-exclusion peak of a VW18 sample immediately after its dissolution in buffer, that is, still in the soluble state, revealed a retention time that ranged between those of typical trimers (pure VW01 sample) and monomers (pure VW01-ran sample) (Figure 6). Evidently, at that early time point, higher oligomers or protofibrils had not yet formed. For VW18/VW01 mixtures with r[18/01] = 1 and 2, that is, under conditions for which the ThT-assay showed almost complete inhibition, only one elution peak was detected in each SEC experiment. This suggested that a single peptide

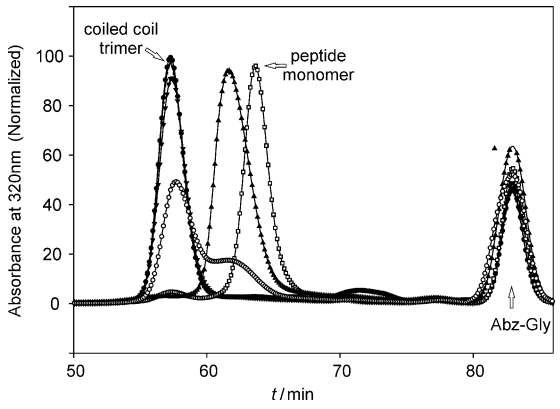

Figure 6. Size-exclusion chromatography scans of VW01, VW01-ran, VW18, and different mixtures as indicated. Abz-Gly was added as a calibration standard.

complex was formed in a particular process of cooperative folding. Moreover, these peaks had the same retention time as the pure trimeric peptide VW01, clearly indicating that these heteromeric complexes comprise trimers. The VW18/VW01 mixture with $r[18/01]=3$ displayed two peaks, a larger one at a retention time similar to that of VW01 and a smaller one at a retention time matching that of the unaggregated VW18 sample. Evidently, the peptide VW01 was no longer able to assemble all VW18 molecules into stable heteromeric trimers at this molar ratio. This conclusion is consistent with the kinetic data derived from the ThT fluorescence assay, which indicated incomplete inhibition.

The presented SEC data strongly suggest the formation of stable heteromeric coiled-coil trimers of VW18 and VW01. The formation of coiled-coil complexes is plausible because the recognition motifs of the peptides that are mainly responsible for their oligomerization state are identical in each case. The particular dependence of the SEC scans on the mixing ratio points to trimeric bundles composed of two VW18 helices and one VW01 helix.

Stability towards proteolytic degradation: A common feature of amyloid cores is their relatively high resistance to proteolytic degradation. Proteolytic cleavage generally occurs at solvent-exposed surfaces and flexible regions of a peptide, while compact hydrogen-bond-stabilized regular structures such as α-helices and β-sheets remain intact.[70] The amyloid core in particular shows resistance towards proteolytic cleavage because of its tightly packed β-strands. By adding different proteases to amyloid aggregates it is therefore possible to obtain valuable information regarding their structural features and dynamics. In various studies, limited proteolysis has been applied to analyze aspects of fibril formation by several amyloidogenic proteins, including Aβ peptide,[71] α-synuclein,[72] and PI3-SH3.[73]

We have investigated the stabilities of the pure model peptides VW18 and VW01 as well as of the respective 2:1 complexes towards proteolytic digestion by incubation with the proteolytic enzyme trypsin. Trypsin has a strong preference for basic amino acids, cleaves peptide bonds C-terminal to lysines and arginines, and has previously demonstrated sensitivity towards the structure of the target amyloid-forming peptide.[71] It is therefore well-suited for the present peptides VW18 and VW01 because their primary sequences contain seven evenly distributed lysine residues. All proteolysis experiments were performed on samples containing 100 μM peptide at pH 7.4 and 37 °C using trypsin at a weight ratio of r[peptide/enzyme]=25. The tryptic peptide digestion reaction was followed by HPLC analysis. The kinetic results displayed in Figure 7 correspond only to the reduction of the total amount of the full-length peptide at the specific retention time; the peaks of the released fragments were not taken into account for the analysis (Figure S9 in the Supporting Information).

The significant difference between the susceptibility to protease digestion of VW18 in the unaggregated oligomeric state and in the aggregated fibrillar state is obvious. Under the proteolysis conditions used, soluble VW18 was digested rapidly within about 20 min. In contrast, in its amyloidogenic state, only about 10% was reduced after 120 min of tryptic digestion. The coiled-coil assemblies of VW01 and the 2:1 VW18/VW01 mixture were digested in an exponential manner, but more slowly compared to the soluble oligomers of VW18. The times required for complete digestions of VW01 and of the 2:1 VW18/VW01 mixture were 60 and 120 min, respectively. The complex of amyloidogenic VW18 and the inhibitor VW01 was found to be more susceptible to proteolytic digestion than mature fibrils of VW18.

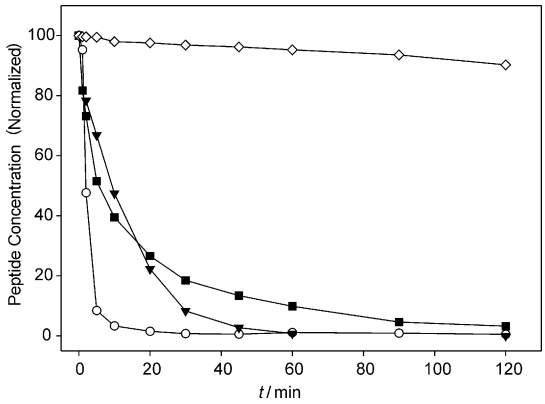

Figure 7. Kinetic data of the proteolysis of VW18 in its aggregated (◇) and soluble state (○), of VW01 alone (▼), and of a 2:1 VW18/VW01 mixture (■) at pH 7.4 and an overall peptide concentration of 100 μM. The single data points are mean values of three independent measurements.

Discussion

CD and ThT fluorescence measurements as well as electron microscopic studies have proved a clear inhibition of VW18 fibrillization by the coiled-coil peptide VW01. Inhibition occurs in a concentration-dependent manner, whereby the effect is nearly complete for $r[18/01]=1$ and $r[18/01]=2$. One has to take into account, however, that all data, including those of the well-established ThT fluorescence method, do not necessarily give quantitative information about fibril formation. Thus, a decreased level of ThT fluorescence could simply result from a partial displacement of dye molecules by the inhibitor.[74,75] The absence of a marked fluorescence decreasing effect of the control peptide VW01-ran, however, rules out this possibility. On the contrary, the strongly different behaviors of the VW01 and VW01-ran peptides seems to emphasize the importance of the coiled-coil recognition motif in the process of inhibition.

Studies on the oligomerization state of the assemblies and the results of inhibition studies, whereby mixtures with $r[18/01]=2$ showed trimeric complexes and complete inhibition, suggest that one inhibitor molecule per two VW18 molecules is necessary to prevent the formation of amyloids. This characteristic ratio points to the formation of stable heterotrimeric coiled-coil complexes caused by complementary in-

teractions between the hydrophobic and electrostatic recognition motifs. Even in the presence of preformed fibrils, which usually nucleate polymerization of the amyloidogenic peptide, the heteromeric complex seems to be sufficiently stable to prevent further aggregation, as the seeding experiments suggested.

It has been reported[29,76–78] that the formation of helical intermediates appears to play an important role in the formation of amyloids. The supposition is that helix-mediated association will lead to high local concentrations of aggregation-prone sequences, which could promote intermolecular β-sheet formation. The heteromeric coiled-coil complex formed between VW18 and VW01 is apparently stable enough to cause just the opposite, that is, to prevent amyloid formation. As expected for a complexation reaction, the degree of inhibition should be a function of the peptide-mixing rate. Indeed, monitoring of the inhibition by ThT binding showed that it first reached completion when the VW01 concentration reached half that of VW18.

The conversion of a coiled coil to a β-sheet trimer has recently been investigated by molecular dynamics (MD) simulations.[79] Two different pathways have been characterized: i) an internal pathway, which involves the direct conversion of α-helices into β-sheet, and ii) a pathway involving dissociation into monomers and their subsequent reassembly into β-sheets. In the MD simulation study of Ito et al. on the unfolding of the central part of the Aβ-peptide (Aβ 13–26) that shows the α/β-discordance, a three-step mechanism was suggested: 1) sufficient loss of helical backbone hydrogen bonds, 2) strong interactions between the nonpolar side chains, and 3) strong interactions between polar side chains. Inhibition of aggregation can occur if one of these steps is not completed.[28] Both studies are consistent with our data and help to rationalize why VW18 undergoes a conformational change and forms amyloid-like fibrils. However, these data also give insights into the mechanism of inhibition.

We can conclude that, due to very strong complementary interactions, the heteromeric helical system formed upon mixing of VW18 and VW01 is too stable to dissociate under the experimental conditions, and thus remains in its fixed helical conformational state. The presence of VW01 in the complex ensures that sufficient helical backbone hydrogen bonds are formed such that the first step of unfolding cannot proceed.

Regarding the stability of differently folded states, computational studies[83] have shown that the β-pleated-sheet structure is the most stable secondary structure element and that there is no thermodynamic reason for aggregation to stop once it has been initiated. The preference for formation of β-pleated sheets arises from strong backbone–backbone interactions, mainly interchain hydrogen bonds. This study has also demonstrated that dimeric helices are thermodynamically less stable than two-stranded β-pleated sheets.

Comparison of the thermodynamic stabilities of the two folded states in the present case is difficult. The mixed system appears to be trapped in a thermodynamically less stable non-amyloid conformation formed by the complexation of peptides VW18 and VW01. A similar effect, whereby a single-point mutation converted the highly amyloidogenic human islet amyloid polypeptide into a fibrillization inhibitor, has recently been reported.[80] However, the exact mode of action remains to be determined in both cases.

Compared to the experiments in which the inhibitor VW01 was present from the beginning of incubation, a much higher fraction of VW01 was necessary to disassemble mature VW18 amyloids. This fact might be explained by the high stability of the amyloid state of VW18, which allows only a small fraction of the mature fibrils to be disturbed by the interaction with the inhibitor molecules. Kinetic effects may be excluded as long-term measurement did not show a remarkable decrease in the amount of fibrillar material.

Proteolysis studies revealed differences in the degree of solvent exposure and the dynamics of proteolytic degradation of the soluble and aggregated states of the peptide VW18. Moreover, the data showed that the helical VW18/VW01 complex was much more susceptible to proteolytic digestion than the aggregated pure peptide VW18. Different factors can affect the protease stability of peptides. First, folded states are more resistant to proteolysis than unfolded states. Second, the rate of proteolytic degradation can also depend on whether the folded native state coexists with an unfolded state. Such coexisting states have been discussed for coiled-coil peptides[81,82] as well as for amyloids.[65,66] Generally, the equilibrium shifts towards the folded native state, but a small fraction of molecules exists in the unfolded state. Only this small fraction is most susceptible to degradation and hence influences the rate of proteolysis. Therefore, the observed significant differences in the proteolysis rates between the coiled-coil and amyloid states might reflect different amounts of coexisting unfolded material rather than pointing to different thermodynamic stabilities of the folded states.[83] The rate of proteolysis can also depend upon the conformation of the folded state. Computer modeling experiments have shown that a local rearrangement is necessary for the substrate to bind to the active site of the enzyme.[73] The rearrangement is relatively easy for helices, but not for extended β-sheet structures, because in the latter case too many hydrogen bonds need to be broken. Both aspects, that is, the amount of the unfolded state as well as the different conformation of the folded state, lead to the conclusion that the β-sheet-rich amyloid state of VW18 is more stable to proteolysis than its helical state, which is consistent with our findings from the proteolysis assay.

Overall, these results suggest how a general approach of inhibiting amyloid formation by targeting the helical elements in the sequence may work in vivo. Preventing the formation of β-sheet-rich amyloid-like structures by specifically stabilizing the helical state of a protein would make the amyloid-forming sequence more susceptible to degradation by proteases and thereby lead to a rapid reduction in amyloidogenic peptide sequences in the cell. A helical inhibitor peptide that is resistant to proteolytic digestion itself would be able to make an excess of amyloidogenic sequences more susceptible to proteolytic digestion.

Conclusion

Using simple de novo designed model peptides, we have studied the fibril aggregation inhibitory activity of a helical peptide. In contrast to other concepts of inhibition, the present peptide-based inhibitor was designed to not disrupt the β-sheet structure of the amyloid core but rather to target the helical elements in the primary structure of the amyloidogenic peptide. In this way, the amyloid-forming target peptide became engaged in a heteromeric helical arrangement through cooperative folding. The formed heteromeric complexes were sufficiently strong to maintain the amyloidogenic sequence in a helical conformation even when the aggregating peptide solution containing the inhibitor peptide was seeded with preformed fibrils. These data suggest that the strategy of designing inhibitors that target the α/β-discordance is effective. It might be a promising approach to interfere with amyloid formation of peptides and proteins that have helical elements in their sequence. The α/β-discordance, which has been described for some naturally occurring amyloidogenic peptides, along with the fact that in some cases helical intermediates are present during amyloid formation, could be used for the development of peptide-based inhibitors capable of serving as strong partners for helix formation. Further studies with naturally occurring amyloidogenic peptides will be necessary to establish the therapeutic potential of this approach.

Experimental Section

Peptide synthesis and purification: All peptides were synthesized by standard Fmoc chemistry on an automated Multi-Syntech Syro XP peptide synthesizer (MultiSynTech, GmbH, Witten, Germany) with Fmoc-Leu-O-Wang resin (0.64 mmol g^{-1}) on a 0.05 mM scale. Standard coupling was carried out with a four-fold excess of amino acids and coupling reagents (TCTU/HOBt) and an eight-fold excess of diisopropylethylamine (DIEA) relative to the loading of the resin. The coupling mixture also contained 0.23 M $NaClO_4$ to prevent on-resin aggregation, especially in the case of the aggregating peptide. Amino acids were coupled two times for 30 min each. The peptides were N-terminally labeled with anthranilic acid (Abz) for photometric determination of the peptide concentration in solution. The peptides were cleaved from the resin by a solution consisting of triisopropylsilane (10% w/v), water (1% w/v), and trifluoroacetic acid (89% w/v). The crude peptide was purified by reversed-phase HPLC using a Knauer Smartline manager 5000 system (Kauer GmbH, Berlin, Germany) with a C8 (10 μm) Phenomenex LUNATM column (Phenomenex Inc., Torrance, CA, USA). Peptides were eluted with a linear gradient of water/acetonitrile/0.1% trifluoroacetic acid. The molecular weights of all peptides were determined by ESI-ToF MS on an Agilent 6210 ESI-ToF LC-mass spectrometer (Agilent Technologies Inc., Santa Clara, CA, USA). The purities of the peptides were determined by analytical HPLC on a Merck LaChrome Elite system (Merck, KGaA, Darmstadt, Germany) with a C8 (10 μm) Phenomonex LUNATM column (Phenomenex Inc., Torrance, CA, USA) and similar solvent gradients to those used for the preparative HPLC.

Sample preparation: The purified non-amyloidogenic peptides were dissolved in freshly prepared and filtered phosphate buffer (10 mM, pH 7.4, 0.1% NaN_3). The peptide concentration, c, was determined by comparing the absorbance measured on a Varian Cary 50 spectrophotometer (Varian Medical Systems, Palo Alto, CA, USA) at $\lambda = 320$ nm with a calibration curve determined by the absorbance of Abz-Gly-OH at different concentrations in the corresponding buffer. Polymethylmethacrylate (PMMA) cuvettes (1.5 mL, Plastibrand, VWR International GmbH, Darmstadt, Germany) were used for the absorption measurements. The lyophilized amyloidogenic peptide VW18 was first dissolved in hexafluoroisopropanol (HFIP) (1 mg mL^{-1}) and then the solution was briefly sonicated and vortexed. The peptide concentration was determined by absorption spectroscopy. The HFIP was then removed under a gentle stream of argon. Thereafter, either pure freshly prepared and filtered phosphate buffer (10 mM, pH 7.4, 0.1% NaN_3) or peptide solutions of VW01 and VW01-ran at different concentrations in phosphate buffer (10 mM, pH 7.4, 0.1% NaN_3) were added.

CD spectroscopy: CD spectra were recorded at 20 °C on a J-810 spectrophotometer (Jasco GmbH, Gross-Umstadt, Germany) using quartz cuvettes (Suprasil, Hellma, Germany) of path length $l = 1$ mm. One spectrum represents the average of three scans in the far-UV region from $\lambda = 240$ to 190 nm. The spectra were corrected for the buffer spectrum and converted into molar ellipticity per residue, $[\Theta]$, according to the equation $[\Theta] = \Theta_{obs}/(10000 \times l \times c \times n)$ with $n = 27$ (including the N-terminal label Abz).

ThT assay: ThT (obtained from Sigma–Aldrich) was used after purification by reversed-phase column chromatography. Fluorescence spectra were measured on a luminescence spectrometer LS50B (Perkin–Elmer, Boston, MA, USA) from solutions in quartz cuvettes (1.4 mL, 10 × 2 mm^2). Samples containing peptide mixture were dissolved in 480 μL of phosphate buffer (10 mM, pH 7.4, 0.1% NaN_3) to which 20 μM of ThT had been added. Each spectrum was measured by accumulating ten scans from $\lambda = 470$ to 600 nm at an excitation wavelength of $\lambda = 450$ nm. Kinetic aggregation curves were generated from time traces of ThT fluorescence intensity at $\lambda = 485$ nm and corrected for the contribution of the free dye.

SEC: Size-exclusion chromatography was performed on an Elite LaChrome System from Hitachi using a Superdex 75 PC 3.2/30 column with a gel volume of 2.4 mL, which was eluted with 100 mM phosphate buffer (pH 7.4), and the absorption of the eluent was monitored at $\lambda = 320$ nm (corresponding to the absorption of the Abz group). The column was equilibrated with phosphate buffer (10 mM, pH 7.4, 0.1% NaN_3). Freshly prepared samples of the pure peptides VW18, VW01, VW01-ran, and VW18/VW01 mixtures were loaded onto the column and eluted with buffer by applying a flow rate of 0.025 mL over 240 min. As a calibration standard, a glycine residue labelled with anthranilic acid (Abz-Gly) was added to each solution.

Analytical ultracentrifugation: Analytical ultracentrifugation (AUC) was performed at 25 °C on an XL-I (Beckman-Coulter, Palo Alto, CA) ultracentrifuge equipped with UV/Vis absorption optics and standard 12 mm double-sector center pieces. Peptide solutions were dialyzed against 10 mM phosphate buffer (10 mM, pH 7.4, 0.1% NaN_3) for four days. Sedimentation velocity experiments were performed at a rotor speed of 60000 rpm and sample concentrations of 20 μM and 300 μM. Sedimentation equilibrium experiments were performed at rotor speeds of 25000, 30000, and 50000 rpm at varying concentrations from 20 to 500 μM. Scanning wavelengths of 320–360 nm were used. Partial specific volume was determined as 0.736 mL g^{-1} by means of a Paar DMA 5000 density meter (Anton Paar, Graz, Austria). Apparent (i.e., for a given loading concentration) weight-average molar masses, $M_{w,app.}$, were determined using the model-independent MSTAR procedure of Harding and Coelfen. The sedimentation velocity data were analyzed using the program SEDFIT of Schuck, yielding the diffusion-corrected molecular mass distribution, c [M].

Electron microscopy: Samples for staining electron microscopy were prepared by absorbing 7 μL aliquots of peptide solution onto glow-discharged carbon-coated collodium films on 400-mesh copper grids. The grids were blotted, stained with 1% phosphotungstic acid (PTA), and air-dried. TEM micrographs were acquired at a primary magnification of 58300 × using a defocus of 0.8 μm. Samples for cryo-TEM were prepared by placing a 10 μL droplet of peptide solution onto a hydrophilized perforated carbon-film covered grid (60 s plasma treatment at 8 W using a BALTEC MED 020 device) at room temperature. To obtain an ultra-thin layer of the sample solution spanning the holes of the carbon film, the supernatant fluid was removed with filter paper. The grids were immediate-

ly vitrified in liquid ethane at its freezing point (−184 °C) using a standard plunging device. The vitrified samples were transferred under liquid nitrogen to a Philips CM12 transmission electron microscope using a Gatan cryo holder and stage (model 626). Microscopy was carried out at a sample temperature of −175 °C by using the low-dose protocol of the microscope at a primary magnification of 58300× with a defocus of 1.5 μm.

Peptide digestion: The samples contained first peptide at a total concentration of 150 μM and were prepared in phosphate buffer (10 mM, pH 7.4, 0.1 % NaN_3). By adding the enzyme stock solution the peptide concentration was diluted to 100 μM. All samples were incubated at 37 °C. After a definite incubation time, the reaction was stopped by adding acetonitrile (0.1 % TFA) and the solutions were diluted with 1 % aqueous TFA to a final peptide concentration of 33 μM. This procedure was necessary to dissolve any fibril, to deactivate the protease, and to prevent further fibril formation in the autosampler of the HPLC. The samples were analyzed by analytical HPLC using a Merck LaChrome Elite system (Merck, KGaA, Darmstadt, Germany) equipped with a Merck Chromolith HPLC column (Merck, KGaA, Darmstadt, Germany). Peptides were eluted with a linear gradient of water/acetonitrile/0.1 % trifluoroacetic acid. The peptide concentration was determined by comparing the calculated HPLC peak area at $\lambda = 220$ nm with a calibration curve determined by calculating the HPLC peak area of a standard peptide of the same length at different, pre-determined by UV, concentrations in the corresponding buffer.

TANGO and AGADIR prediction: The online software TANGO (http://tango.crg.es/) and AGADIR (http://agadir.crg.es/) were used to obtain sequence-dependent aggregation and helicity profiles of the amyloidogenic peptide VW18 and the coiled-coil peptide VW01.

Acknowledgements

The authors thank A. Völkel (MPI-KGF, Potsdam-Golm) for her very kind assistance with the ultracentrifugation experiments and A. Berger and P. Winchester for proofreading of the manuscript. We are grateful for financial support from the Deutsche Forschungsgemeinschaft (KO 1976/5 and BO 1000/7).

[1] F. Chiti, C. M. Dobson, *Nat. Chem. Biol.* **2009**, *5*, 15–22.
[2] F. Chiti, C. M. Dobson, *Annu. Rev. Biochem.* **2006**, *75*, 333–366.
[3] C. M. Dobson, *Nature* **2003**, *426*, 884–890.
[4] S. Baglioni, F. Casamenti, M. Bucciantini, L. M. Luheshi, N. Taddei, F. Chiti, C. M. Dobson, M. Stefani, *J. Neurosci.* **2006**, *26*, 8160–8167.
[5] R. Kayed, E. Head, J. L. Thompson, T. M. McIntire, S. C. Milton, C. W. Cotman, C. G. Glabe, *Science* **2003**, *300*, 486–489.
[6] P. T. Lansbury, H. A. Lashuel, *Nature* **2006**, *443*, 774–779.
[7] D. M. Walsh, I. Klyubin, J. V. Fadeeva, M. J. Rowan, D. J. Selkoe, *Biochem. Soc. Trans.* **2002**, *30*, 552–557.
[8] B. Caughey, P. T. Lansbury, *Annu. Rev. Neurosci.* **2003**, *26*, 267–298.
[9] D. M. Walsh, D. J. Selkoe, *Protein Pept. Lett.* **2004**, *11*, 213–228.
[10] B. Y. Feng, B. H. Toyama, H. Wille, D. W. Colby, S. R. Collins, B. C. H. May, S. B. Prusiner, J. Weissman, B. K. Shoichet, *Nat. Chem. Biol.* **2008**, *4*, 197–199.
[11] H. LeVine III, *Amyloid* **2007**, *14*, 185–197.
[12] S. M. Chafekar, H. Malda, M. Merkx, E. W. Meijer, D. Viertl, H. A. Lashuel, F. Baas, W. Scheper, *ChemBioChem* **2007**, *8*, 1857–1864.
[13] N. Kokkoni, K. Stott, H. Amijee, J. M. Mason, A. J. Doig, *Biochemistry* **2006**, *45*, 9906–9918.
[14] K. L. Sciarretta, D. J. Gordon, S. C. Meredith, *Methods Enzymol.* **2006**, *413*, 273–312.
[15] A. D. Williams, M. Sega, M. Chen, I. Kheterpal, M. Geva, V. Berthelier, D. T. Kaleta, K. D. Cook, R. Wetzel, *Proc. Natl. Acad. Sci. USA* **2005**, *102*, 7115–7120.
[16] J. M. Mason, N. Kokkoni, K. Stott, A. J. Doig, *Curr. Opin. Struct. Biol.* **2003**, *13*, 526–532.
[17] J. Madine, A. J. Doig, D. A. Middleton, *J. Am. Chem. Soc.* **2008**, *130*, 7873–7881.
[18] C. K. Bett, J. N. Ngunjiri, W. K. Serem, K. R. Fontenot, R. P. Hammer, R. L. McCarley, J. C. Garno, *ACS Chem. Neurosci.* **2010**, *1*, 661–678.
[19] T. J. Gibson, R. M. Murphy, *Biochemistry* **2005**, *44*, 8898–8907.
[20] M. Bartolini, C. Bertucci, M. L. Bolognesi, A. Cavalli, C. Melchiorre, V. Andrisano, *ChemBioChem* **2007**, *8*, 2152–2161.
[21] T. R. Foss, M. S. Kelker, R. L. Wiseman, I. A. Wilson, J. W. Kelly, *J. Mol. Biol.* **2005**, *347*, 841–854.
[22] F. E. Cohen, J. W. Kelly, *Nature* **2003**, *426*, 905–909.
[23] D. E. Ehrnhoefer, J. Bieschke, A. Boeddrich, M. Herbst, L. Masino, R. Lurz, S. Engemann, A. Pastore, E. E. Wanker, *Nat. Struct. Mol. Biol.* **2008**, *15*, 558–566.
[24] Y. Kallberg, M. Gustafsson, B. Persson, J. Thyberg, J. Johansson, *J. Biol. Chem.* **2001**, *276*, 12945–12950.
[25] M. D. Kirkitadze, M. M. Condron, D. B. Teplow, *J. Mol. Biol.* **2001**, *312*, 1103–1119.
[26] D. B. Teplow, N. D. Lazo, G. Bitan, S. Bernstein, T. Wyttenbach, M. T. Bowers, A. Baumketner, J. E. Shea, B. Urbanc, L. Cruz, J. Borreguero, H. E. Stanley, *Acc. Chem. Res.* **2006**, *39*, 635–645.
[27] M. Dasari, A. Espargaro, R. Sabate, J. M. Lopez Del Amo, U. Fink, G. Grelle, J. Bieschke, S. Ventura, B. Reif, *ChemBioChem* **2011**, *12*, 407–423.
[28] M. Ito, J. Johansson, R. Stromberg, L. Nilsson, *PLoS One* **2011**, *6*, e17587.
[29] J. A. Williamson, J. P. Loria, A. D. Miranker, *J. Mol. Biol.* **2009**, *393*, 383–396.
[30] G. Liu, A. Prabhakar, D. Aucoin, M. Simon, S. Sparks, K. J. Robbins, A. Sheen, S. A. Petty, N. D. Lazo, *J. Am. Chem. Soc.* **2010**, *132*, 18223–18232.
[31] R. Kunjithapatham, F. Y. Oliva, U. Doshi, M. Perez, J. Avila, V. Munoz, *Biochemistry* **2005**, *44*, 149–156.
[32] V. L. Anderson, T. F. Ramlall, C. C. Rospigliosi, W. W. Webb, D. Eliezer, *Proc. Natl. Acad. Sci. USA* **2010**, *107*, 18850–18855.
[33] F. Fiumara, L. Fioriti, E. R. Kandel, W. A. Hendrickson, *Cell* **2010**, *143*, 1121–1135.
[34] G. D'Auria, M. Vacatello, L. Falcigno, L. Paduano, G. Mangiapia, L. Calvanese, R. Gambaretto, M. Dettin, L. Paolillo, *J. Pept. Sci.* **2009**, *15*, 210–219.
[35] A. Abedini, D. P. Raleigh, *Protein Eng. Des. Sel.* **2009**, *22*, 453–459.
[36] I. Saraogi, J. A. Hebda, J. Becerril, L. A. Estroff, A. D. Miranker, A. D. Hamilton, *Angew. Chem.* **2010**, *122*, 748–751; *Angew. Chem. Int. Ed.* **2010**, *49*, 736–739.
[37] J. Li, R. Liu, K. S. Lam, L. W. Jin, Y. Duan, *Biophys. J.* **2011**, *100*, 1076–1082.
[38] A. Päiviö, E. Nordling, Y. Kallberg, J. Thyberg, J. Johansson, *Protein Sci.* **2004**, *13*, 1251–1259.
[39] C. Nerelius, A. Sandegren, H. Sargsyan, R. Raunak, H. Leijonmarck, U. Chatterjee, A. Fisahn, S. Imarisio, D. A. Lomas, D. C. Crowther, R. Stromberg, J. Johansson, *Proc. Natl. Acad. Sci. USA* **2009**, *106*, 9191–9196.
[40] A. Esteras-Chopo, M. T. Pastor, M. Lopez de la Paz, *Methods Mol. Biol.* **2006**, *340*, 253–276.
[41] M. T. Pastor, A. Esteras-Chopo, M. Lopez de la Paz, *Curr. Opin. Struct. Biol.* **2005**, *15*, 57–63.
[42] R. Mimna, M. S. Camus, A. Schmid, G. Tuchscherer, H. A. Lashuel, M. Mutter, *Angew. Chem.* **2007**, *119*, 2735–2738; *Angew. Chem. Int. Ed.* **2007**, *46*, 2681–2684.
[43] L. J. Page, J. Y. Suk, L. Bazhenova, S. M. Fleming, M. Wood, Y. Jiang, L. T. Guo, A. P. Mizisin, R. Kisilevsky, G. D. Shelton, W. E. Balch, J. W. Kelly, *Proc. Natl. Acad. Sci. USA* **2009**, *106*, 11125–11130.
[44] K. Pagel, S. C. Wagner, K. Samedov, H. von Berlepsch, C. Böttcher, B. Koksch, *J. Am. Chem. Soc.* **2006**, *128*, 2196–2197.
[45] K. Pagel, T. Vagt, T. Kohajda, B. Koksch, *Org. Biomol. Chem.* **2005**, *3*, 2500–2502.

[46] H. von Berlepsch, S. C. Wagner, R. R. Araghi, K. Pagel, J. Leiterer, F. Emmerling, A. Schulz, C. Böttcher, B. Koksch, unpublished results.
[47] K. Pagel, T. Seri, H. von Berlepsch, J. Griebel, R. Kirmse, C. Böttcher, B. Koksch, *ChemBioChem* **2008**, *9*, 531–536.
[48] M. Broncel, J. A. Falenski, S. C. Wagner, C. P. R. Hackenberger, B. Koksch, *Chem. Eur. J.* **2010**, *16*, 7881–7888.
[49] M. Broncel, S. C. Wagner, C. P. R. Hackenberger, B. Koksch, *Chem. Commun.* **2010**, *46*, 3080–3082.
[50] M. Broncel, S. C. Wagner, K. Paul, C. P. R. Hackenberger, B. Koksch, *Org. Biomol. Chem.* **2010**, *8*, 2575–2579.
[51] K. Pagel, S. C. Wagner, R. Rezaei Araghi, H. von Berlepsch, C. Böttcher, B. Koksch, *Chem. Eur. J.* **2008**, *14*, 11442–11451.
[52] P. Burkhard, J. Stetefeld, S. V. Strelkov, *Trends Cell Biol.* **2001**, *11*, 82–88.
[53] J. M. Mason, K. M. Arndt, *ChemBioChem* **2004**, *5*, 170–176.
[54] D. N. Woolfson, *Adv. Protein Chem.* **2005**, *70*, 79–112.
[55] A.-M. Fernandez-Escamilla, F. Rousseau, J. Schymkowitz, L. Serrano, *Nat. Biotechnol.* **2004**, *22*, 1302–1306.
[56] V. Muñoz, L. Serrano, *Nat. Struct. Biol.* **1994**, *1*, 399–409.
[57] F. Rousseau, J. Schymkowitz, L. Serrano, *Curr. Opin. Struct. Biol.* **2006**, *16*, 118–126.
[58] M. T. Pastor, A. Esteras-Chopo, L. Serrano, *Prion* **2007**, *1*, 9–14.
[59] W.-F. Xue, S. W. Homans, S. E. Radford, *Proc. Natl. Acad. Sci. USA* **2008**, *105*, 8926–8931.
[60] F. Ferrone, *Methods Enzymol.* **1999**, *309*, 256–274.
[61] S. F. Betz, W. F. DeGrado, *Biochemistry* **1996**, *35*, 6955–6962.
[62] A. Piñeiro, A. Villa, T. Vagt, B. Koksch, A. E. Mark, *Biophys. J.* **2005**, *89*, 3701–3713.
[63] WINNONLIN v. 1.06, D. A. Yphantis, M. L. Johanson, J. W. Lary, University of Connecticut, **1997**.
[64] H. Cölfen, S. E. Harding, *Eur. Biophys. J.* **1997**, *25*, 333–346.
[65] N. Carulla, G. L. Caddy, D. R. Hall, J. Zurdo, M. Gairi, M. Feliz, E. Giralt, C. V. Robinson, C. M. Dobson, *Nature* **2005**, *436*, 554–558.
[66] B. O'Nuallain, S. Shivaprasad, I. Kheterpal, R. Wetzel, *Biochemistry* **2005**, *44*, 12709–12718.
[67] K. Ono, T. Hamaguchi, H. Naiki, M. Yamada, *Biochim. Biophys. Acta* **2006**, *1762*, 575–586.
[68] L. D. Estrada, C. Soto, *Curr. Top. Med. Chem.* **2007**, *7*, 115–126.
[69] T. Hamaguchi, K. Ono, M. Yamada, *Cell. Mol. Life Sci.* **2006**, *63*, 1538–1552.
[70] A. Fontana, P. P. de Laureto, B. Spolaore, E. Frare, P. Picotti, M. Zambonin, *Acta Biochim. Pol.* **2004**, *51*, 299–321.
[71] I. Kheterpal, A. Williams, C. Murphy, B. Bledsoe, R. Wetzel, *Biochemistry* **2001**, *40*, 11757–11767.
[72] H. Miake, H. Mizusawa, T. Iwatsubo, M. Hasegawa, *J. Biol. Chem.* **2002**, *277*, 19213–19219.
[73] P. Polverino de Laureto, N. Taddei, E. Frare, C. Capanni, S. Costantini, J. Zurdo, F. Chiti, C. M. Dobson, A. Fontana, *J. Mol. Biol.* **2003**, *334*, 129–141.
[74] M. R. Nilsson, *Methods* **2004**, *34*, 151–160.
[75] F. Meng, P. Marek, K. J. Potter, C. B. Verchere, D. P. Raleigh, *Biochemistry* **2008**, *47*, 6016–6024.
[76] A. Abedini, D. P. Raleigh, *Phys. Biol.* **2009**, *6*, 015005.
[77] J. A. Williamson, A. D. Miranker, *Protein Sci.* **2007**, *16*, 110–117.
[78] H. Mihara, Y. Takahashi, *Curr. Opin. Struct. Biol.* **1997**, *7*, 501–508.
[79] B. Strodel, A. W. Fitzpatrick, M. Vendruscolo, C. M. Dobson, D. J. Wales, *J. Phys. Chem. B* **2008**, *112*, 9998–10004.
[80] A. Abedini, F. Meng, D. P. Raleigh, *J. Am. Chem. Soc.* **2007**, *129*, 11300–11301.
[81] A. J. Doig, *Biophys. Chem.* **2002**, *101–102*, 281–293.
[82] T. Wang, W. L. Lau, W. F. DeGrado, F. Gai, *Biophys. J.* **2005**, *89*, 4180–4187.
[83] A. S. Perczel, P. T. Hudaky, V. K. Palfi, *J. Am. Chem. Soc.* **2007**, *129*, 14959–14965.

Received: March 3, 2011
Published online: August 16, 2011

